Available online at www.sciencedirect.com
ScienceDirect
Applied Numerical Mathematics 57 (2007) 510–520
APPLIED NUMERICAL MATHEMATICS
www.elsevier.com/locate/apnum

Model reduction applied to square to rectangular martensitic transformations using proper orthogonal decomposition

L.X. Wang [a,*], Roderick V.N. Melnik [b]

[a] *MCI, Faculty of Science and Engineering, University of Southern Denmark, Sonderborg DK-6400, Denmark*
[b] *Mathematical Modelling & Computational Sciences, Wilfrid Laurier University, 75 University Avenue West, Waterloo, ON, Canada, N2L 3C5*

Available online 9 August 2006

Abstract

Model reduction using the proper orthogonal decomposition (POD) method is applied to the dynamics of ferroelastic patches to study the first-order square to rectangular phase transformations. Governing equations for the system dynamics are constructed by using the Landau–Ginzburg theory and are solved numerically. By using the POD method, a set of empirical orthogonal basis functions is first constructed, then the system is projected onto the subspace spanned by a small set of basis functions determined by the associated singular values. The performance of the low-dimensional model is verified by simulating nonlinear thermo-mechanical waves and square to rectangular transformations in a ferroelastic patch. Comparison between numerical results obtained from the original PDE model and the low-dimensional one is carried out.

Keywords: Phase transformation; Ferroelastic patch; Model reduction; Proper orthogonal decomposition; Galerkin projection

1. Introduction

The first-order martensite transformation is a common transformation in many ferroelastic, ferromagnetic, and ferroelectric materials that holds the key to their specific properties. For many new engineering applications of such materials, a better understanding of the mechanism of the transformation becomes decisively important. As a result, the martensite transformations observed in smart materials have attracted substantial attention from engineers, mathematicians, physicists, and control theorists. These materials possess unique properties of being able to sense, actuate, and inherently respond to external stimuli ([9] and references therein). Much attention is devoted to control and design optimization of these materials where mathematical modeling tools become ubiquitous. However, even for the systems governed by linear partial differential equations (PDE), these issues are far from trivial [8,10]. At the same time, mathematical models describing the dynamic behavior of most smart materials are intrinsically nonlinear, coupling different physical fields by conservation law equations and constitutive relations (e.g., [3,5,12]). To bridge the gap between the nonlinear PDEs such as those arising in the description of the smart material systems and the low-dimensional models suitable for control and optimization in realistic engineering applications, it is natural to attempt to approximate the dynamic behavior of PDEs by low-dimensional models. Such low-dimensional models

* Corresponding address. Tel.: +45 6550 1686; fax: +45 6550 1660.
E-mail address: wanglinxiang@mci.sdu.dk (L.X. Wang).

0168-9274/$30.00
doi:10.1016/j.apnum.2006.07.004

can be obtained from the original systems by model reduction and the POD provides an efficient tool for doing so as soon as a collection of system states is available. This idea has been successfully applied to many active control problems involving fluid flows (see [2,8] and references therein). Recently, we applied this idea to the analysis of phase transformations in the 1D case [13]. In its essence, the POD methodology is close to the principal component analysis, techniques based on the singular value decomposition, and Karhunen–Loeve decomposition [2,8].

In this paper, we develop a low-dimensional model for the dynamics of ferroelastic patches exhibiting square to rectangular phase transformations to study 2D nonlinear thermomechanical waves. First, the original system of PDEs is analyzed numerically with Chebyshev's collocation method. Then, the basis functions are extracted from the obtained numerical results using the POD. Finally, the low-dimensional model is constructed using the Galerkin projection method. The dynamic behavior of ferroelastic patches is simulated by the empirical low-dimensional model, and its performance is evaluated by comparing the numerical results with those from the original PDE model.

2. PDE model and its numerical solution

Square to rectangular transformations are regarded as a 2D analog of the cubic to tetragonal or tetragonal to orthorhombic transformations observed in the general 3D case (see, e.g., [3] and reference therein). At mesoscale, there is a high temperature phase of greater symmetry (austenite, represented schematically as square), and two lower temperature phases (martensite variants, represented schematically as rectangles). The transformation from austenite to martensite is not unique due to the fact that there are multiple equivalent orientations of the lower symmetry lattice with respect to the parent lattice.The transformation can be induced by either mechanical or thermal loadings (or their combination), but only mechanically induced transformation will be modeled here.

The governing equations describing the macroscopic dynamics of the ferroelastic structure exhibiting the above mentioned transformation can be formulated on the basis of conservation laws. Following [12], we consider the following coupled system of PDEs based on conservation of momentum and energy:

$$
\begin{aligned}
&\frac{\partial^2 u_1}{\partial t^2} = \frac{\partial \sigma_{11}}{\partial x} + \frac{\partial \sigma_{12}}{\partial y} + f_x, \qquad \frac{\partial^2 u_2}{\partial t^2} = \frac{\partial \sigma_{12}}{\partial x} + \frac{\partial \sigma_{22}}{\partial y} + f_y,\\
&c_v \frac{\partial \theta}{\partial t} = k\left(\frac{\partial^2 \theta}{\partial x^2} + \frac{\partial^2 \theta}{\partial y^2}\right) + a_2 \theta e_2 \frac{\partial e_2}{\partial t} + g,\\
&\sigma_{11} = \frac{\sqrt{2}}{2}\rho\left(a_1 e_1 + a_2(\theta - \theta_0)e_2 - a_4 e_2^3 + a_6 e_2^5\right) + \frac{d_2}{2}\nabla_x^2 e_2,\\
&\sigma_{12} = \frac{1}{2}\rho a_3 e_3 = \sigma_{21},\\
&\sigma_{22} = \frac{\sqrt{2}}{2}\rho\left(a_1 e_1 - a_2(\theta - \theta_0)e_2 + a_4 e_2^3 - a_6 e_2^5 + \frac{d_2}{2}\nabla_y^2 e_2\right),
\end{aligned}
\tag{1}
$$

where c_v is the specific heat constant, θ_0 is the reference temperature for the transformation, ∇ is the gradient operator, a_1, a_2, a_3, a_4, a_6, and d_2 are the material-specific coefficients, and e_1, e_2, e_3 are dilatational, deviatoric, and shear components of the strains, respectively. f_x, f_y and g are mechanical and thermal loadings, respectively.

In the above model, e_2 is chosen as the only order parameter to characterize differences in phases. Strain components are defined as follows:

$$
e_1 = (\eta_{11} + \eta_{22})/\sqrt{2}, \qquad e_2 = (\eta_{11} - \eta_{22})/\sqrt{2}, \qquad e_3 = (\eta_{12} + \eta_{21})/2, \tag{2}
$$

where the Cauchy–Lagrangian strain tensor $\boldsymbol{\eta}$ is given by its components as follows (with the repeated-index convention used):

$$
\eta_{ij}(\mathbf{x}, t) = \left(\frac{\partial u_i(\mathbf{x}, t)}{\partial x_j} + \frac{\partial u_j(\mathbf{x}, t)}{\partial x_i}\right)\Big/ 2. \tag{3}
$$

In the above formulation, stress components are kept as independent variables to be solved for. This approach is similar to the DAE approach first proposed in the context of shape memory alloys materials modeling in [5].

2.1. Chebyshev collocation methodology

The system formulated in the previous section is solved here numerically by the method of lines. First, we discretize the system spatially, converting it into a system of differential-algebraic equations, and then we apply a backward differential formula to integrate the resulting system in time.

For the spatial discretization, the Chebyshev pseudospectral approximation is employed on a set of 2D Chebyshev points $(x_i, y_j) \in [-1, 1] \times [-1, 1]$ [1]:

$$x_i = \cos\left(\frac{\pi i}{N}\right), \qquad y_j = \cos\left(\frac{\pi j}{N}\right), \quad i, j = 0, 1, \ldots, N, \tag{4}$$

where $N + 1$ is the number of nodes. Using the discretization, all the unknown distributions in the patch can be approximated by the following linear combination:

$$f(x, y) = \sum_{i=0}^{N} \sum_{j=0}^{N} f_{i,j} \phi_i(x) \phi_j(y), \tag{5}$$

where $f(x, y)$ could be either stresses, displacements, velocities, or temperature; $f_{i,j}$ is the function value at (x_i, y_j); $\phi_i(x)$ and $\phi_j(y)$ are the ith and jth Lagrange interpolating polynomials in x and y directions, respectively.

Because Eq. (5) is just a linear combination of the interpolating polynomials, the derivatives of the functions $\partial f(x, y)/\partial x$ and $\partial f(x, y)/\partial y$ can be easily obtained by calculating $\partial \phi_i(x)/\partial x$ and $\partial \phi_j(y)/\partial y$. Following the idea given in [11], all the differential operators in Eq. (1) can be written as a matrix form:

$$\left.\frac{\partial f(x, y)}{\partial x}\right|_{x_i, y_j} = \boldsymbol{D}_x \boldsymbol{F}, \qquad \left.\frac{\partial f(x, y)}{\partial y}\right|_{x_i, y_j} = \boldsymbol{D}_y \boldsymbol{F}, \tag{6}$$

and similarly for the higher-order differentiation operators. The differentiation matrices $\boldsymbol{D}_x$, $\boldsymbol{D}_y$, $\boldsymbol{D}_{xx}$, and $\boldsymbol{D}_{yy}$ can be calculated using the approximation given by Eq. (5).

By approximating all the differential operators in the governing Eq. (1), the system can be discretized and converted into a set of nonlinear ODEs and algebraic equations. The boundary conditions of the system can be easily enforced [11,1]. The system after discretization finally takes the following form:

$$\boldsymbol{M} \frac{\mathrm{d}\boldsymbol{X}}{\mathrm{d}t} + \boldsymbol{G}(t, \boldsymbol{X}, \boldsymbol{U}) = 0, \tag{7}$$

where $\boldsymbol{X}$ is a $5(N+1)$ vector collecting all the unknowns we are seeking for, the matrix $\boldsymbol{M} = \mathrm{diag}(a_1, a_2, \ldots, a_{5(N+1)})$ is a $5(N + 1) \times 5(N + 1)$ matrix having entries "one" for all the differential equations associated with ODEs and "zero" for all algebraic equations.

The above DAEs system is a stiff system and must be solved by an implicit algorithm. Here, the second-order backward differentiation formula method is employed for this purpose. By discretizing the time derivative using the second-order approximation, the DAE system can be converted into the following algebraic system at each time level:

$$\boldsymbol{M}\left(\frac{3}{2}\boldsymbol{X}^n - 2\boldsymbol{X}^{n-1} + \frac{1}{2}\boldsymbol{X}^{n-2}\right) + \Delta t \boldsymbol{N}\big(t_n, \boldsymbol{X}^n, \boldsymbol{V}(t_n)\big) = 0, \tag{8}$$

where n denotes the current computational time layer. For each computational time layer, iterations are carried out with the bi-conjugated gradient iteration method for computing $\boldsymbol{X}^n$ having $\boldsymbol{X}^{n-1}$ and $\boldsymbol{X}^{n-2}$. Starting from the initial value, the vector of unknowns $\boldsymbol{X}$ is sought for all specified time instances employing this algorithm.

We note that to deal with strong (cubic and quintic) nonlinearities in the order parameter, a smoothing procedure similar to that proposed in [6] has been employed during the iteration process. In particular, we have used the following expansions:

$$y^3 = \frac{1}{4} \sum_{i=0}^{3} y_n^i y_{n-1}^{3-i}, \qquad y^5 = \frac{1}{6} \sum_{i=0}^{5} y_n^i y_{n-1}^{5-i}, \tag{9}$$

where y stands for e_2 here, and n time layer.

3. Construction of low-dimensional models

3.1. Proper orthogonal decomposition

One of the most effective ways to construct a low-dimensional model for approximation to a dynamical system is to find a set of optimal basis functions by which the dynamical system can be approximated best at any time. In what follows, we apply the POD method to construct an empirical basis for the system dynamics describing 2D phase transformations.

For the dynamical system given by Eq. (1), the system state at any time can be fully characterized by the displacements, velocity, and temperature distributions, while displacements and velocities can be represented by using the same basis functions. Here, we only need to construct spatial basis functions for displacement and temperature distributions. Let us assume that $\mathcal{U}(x,t)$, which describes the system dynamics, belongs to an inner product (Hilbert) space $\mathcal{H}$. The POD is concerned with the possibility to find a set of orthonormal spatial basis functions $\phi = \{\phi_j(x),\ j = 1,\ldots,P\}$ in $\mathcal{H}$ which are optimal in the sense that the P-dimensional approximation

$$\mathcal{U}_P(x,t) = \sum_{i=1}^{P} a_i(t)\phi_i(x) \tag{10}$$

gives the best (in the least square sense) approximation to the function $\mathcal{U}(x,t)$ among all those P-dimensional approximations in $\mathcal{H}$ [2,7]. Here a_i are the general Fourier coefficients associated with $\{\phi_i\}$. They are functions of time. Mathematically, the idea of POD is to choose the basis functions $\{\phi_k\}$ to maximize the mean projection of the function $\mathcal{U}(x,t)$ on $\{\phi_k\}$

$$\max_{\phi\in L_2(\Omega)} \frac{E(|\langle \mathcal{U},\phi\rangle|^2)}{\|\phi\|^2}, \tag{11}$$

where $E(\cdot)$ denotes the mean value functional, $|\cdot|$ is the modulus, $\langle\cdot\rangle$ is the inner product, and $\|\cdot\|$ is the L^2 norm [2,7].

For convenience of the projection operation, that will be employed later, the orthonormality requirement is enforced on the basis functions we are looking for:

$$\langle \phi_i, \phi_j\rangle = \begin{cases} 1 & \text{if } i = j, \\ 0 & \text{if } i \neq j. \end{cases} \tag{12}$$

The general Fourier coefficients in this case can be calculated simply as:

$$a_i(t) = \big\langle \mathcal{U}(x,t), \phi_i \big\rangle. \tag{13}$$

Taking into account the above requirement on the basis functions, the maximization problem can be reformulated in terms of calculus of variation, with a functional for the constrained variational problem [2,7]:

$$J[\phi] = E\big(\big|\langle \mathcal{U},\phi\rangle\big|^2\big) - \lambda\big(\|\phi\|^2 - 1\big). \tag{14}$$

A necessary condition for extrema is that the first-order variation of the functional with respect to all variations $\phi + \delta\psi$ should be zero:

$$\frac{\partial}{\partial\delta} J[\phi + \delta\psi]|_{\delta=0} = 0, \tag{15}$$

which finally leads to the following eigenvalue problem [2,7]:

$$\int_{\Omega} E\big(\mathcal{U}(x)\mathcal{U}(x')\big)\phi(x')\,\mathrm{d}x' = \lambda\phi(x), \tag{16}$$

whose kernel $\mathcal{K} = E(\mathcal{U}(x)\mathcal{U}(x'))$ is the auto-covariance function of the two points x and x'.

For the current problem, the dynamics of the system can be sampled at any time instances we need, by using the numerical algorithm mentioned above for Eq. (1). Let us denote by U^i the system state at the ith time instance, called the ith snapshot. In discrete form, each snapshot can be written as a column vector with M entries, where M is the number of nodes for spatial discretization.

To construct the orthonormal basis, all the snapshots are collected in one matrix $U = \{U^i,\ i = 1, \ldots, N\}$. If one put each snapshot as one column in the collection matrix, the collection U will be a matrix of $M \times N$. The orthonormal basis vectors for the given collection U can be calculated by the singular value decomposition as follows:

$$U = LSR^T, \tag{17}$$

where L is $M \times M$ orthonormal matrix, R is a $N \times N$ orthonormal matrix and the superscripts T indicates matrix transpose. S is a $M \times N$ matrix with all elements zero except along the diagonal, those nonzero elements are arranged in a decreasing way along the diagonal. They are the singular values of U, emphasizing the relative importance of its associated eigenvectors in L and R.

Let $SR^T = Q^T$ in the singular value decomposition, then $U = LQ^T$. Let ϕ_k be the kth column of L and a_k be the kth row of Q, then the matrix U's singular value decomposition can be rewritten as

$$U = \sum_{k=1}^{m} a_k \phi_k, \tag{18}$$

where $m = \min(N, M)$ is the rank of the collection matrix U. This approximation is what we are looking for in Eq. (10). The lower-dimensional approximation of the matrix U can be easily obtained by keeping the first few largest singular values and their associated eigenvectors in L and Q. The number of eigenvectors should be determined by compromising between the dimension number of the resultant system and the approximation accuracy [7,2].

3.2. Galerkin projection

It has already been mentioned that Eq. (1) can be converted into a system of DAEs like Eq. (7) by discretization. It can also be converted into a system of ODEs if we substitute all the constitutive relations into Eq. (1). The latter approach is applied here for the construction of the low-dimensional model. For convenience, Eq. (1) is converted into a dynamical system representation as follows:

$$\frac{\mathrm{d}}{\mathrm{d}t}\boldsymbol{X} = \boldsymbol{Q}(t, \boldsymbol{X}, \boldsymbol{H}), \tag{19}$$

where $\boldsymbol{Q}$ is the collection of functions given by the spatial discretization of Eq. (1), while $\boldsymbol{H}$ is the collection of inputs after conversion. Vector $\boldsymbol{x}$ collects all unknowns including displacements in the x and y directions, velocities in the x and y directions, and temperatures in the collocation nodes.

Having obtained the optimal basis functions for the dynamical system, its lower-dimensional approximation can be obtained by projecting the full system orthogonally onto the subspace spanned by the chosen basis functions. It is known that the model reduction can be achieved due to the fact that much smaller number of basis functions are needed to approximate the full system, when the chosen basis functions are optimal.

Let us denote the projection operator as P_r and P_r^T its transpose. Then, a low-dimensional system on the chosen subspace S can be constructed by using the following rule:
For any point $\boldsymbol{Z} \in S$, compute the vector field $\boldsymbol{Q}(t, \boldsymbol{H}, P_r^T \boldsymbol{Z})$ and take the projection $P_r Q(t, \boldsymbol{H}, P_r^T \boldsymbol{Z})$ on to the subspace S. It should be equal to $\dot{\boldsymbol{Z}}$. The result can be formulated as:

$$\frac{\mathrm{d}}{\mathrm{d}t}\boldsymbol{Z} = P_r \boldsymbol{Q}\big(t, P_r^T \boldsymbol{Z}, \boldsymbol{H}\big). \tag{20}$$

The approximation will introduce an error defined as follows:

$$r = \boldsymbol{X} - P_r^T \boldsymbol{Z}. \tag{21}$$

To achieve the best approximation with the given basis, the error function of the approximation is required to be orthogonal to all the basis functions at any time:

$$(r, \phi_k) = \int_{\Omega} r(x)\phi(x)\,\mathrm{d}x = 0. \tag{22}$$

It is easy to check that the low-dimensional system given by Eq. (20) satisfies this condition, if the orthogonality of the basis functions is used.

4. Numerical results

To demonstrate the performance of the proposed methodology, numerical results from the low-dimensional model for the dynamics of a ferroelastic patch are compared with its counterparts from the PDE model. The dynamical behavior of a $Au_{23}Cu_{30}Zn_{47}$ patch with size of $[0, 1] \times [0, 1]$ cm^2 is analyzed numerically. All the physical parameters for this specific material are available in the literature (e.g., [4,12]). It has been shown that the first-order square to rectangular transformation can be mechanically induced in this material [4,5,12]. It has also been shown that the nonlinearity is very strong, and the nonlinear coupling between the mechanical and thermal fields complicates the problem further.

The strategy here is as follows:
We first perform the numerical simulation using Eq. (1) with a representative mechanical load. As a result, the collection matrix can be constructed and the empirical eigenfunctions can be extracted. Then, we simulate the dynamics using Eq. (20) with loads that differ from the previous loading. By comparing the numerical results from Eq. (20) with those from Eq. (1), we assess the performance of the low-dimensional model.

The initial conditions for all the simulations reported below are set the same. They are $\theta(x, 0) = 250$ K and $u_1 = u_2 = v_1 = v_2 = 0$. Boundary conditions for Eq. (1) are taken as pinned-end mechanically and insulated thermally. The distributed mechanical loading for collecting snapshots is the following (for one period, $g/(\text{ms}^2\,\text{cm}^2)$)

$$f_x = f_y = \begin{cases} 7000t/2, & 0 \leqslant t \leqslant 2, \\ 7000(4-t)/2, & 2 \leqslant t \leqslant 4, \\ 0, & 4 \leqslant t \leqslant 6, \\ 7000(6-t)/2, & 6 \leqslant t \leqslant 8, \\ 7000(t-10)/2, & 8 \leqslant t \leqslant 10, \\ 0, & 10 \leqslant t \leqslant 12. \end{cases}$$

There are 13 nodes, each used for u_1, u_2, v_1, v_2, and θ discretization. Two periods of loadings are performed ($t \in [0, 24]$) and totally 201 evenly distributed snapshots are sampled. The collection matrix for each field variable then can be constructed by collecting their values on each sampling instance. To demonstrate the phase transformation, the order parameter and temperature on the central horizontal line are plotted versus time in Fig. 1.

With the above constructed collection matrix at hand, the POD for each of the field variables can be done by using Eqs. (17) and (18), by which the eigenfunctions for u_1, u_2, v_1, v_2 and θ can be estimated [13]. The first three eigenfunctions for displacement u_1 are plotted in the left column of Fig. 2, together with those three for temperature in the right column. The eigenfunctions for v_1 can be taken as the same as those for u_1 because their differences are in time domain, and similar for v_2.

For the construction of the low-dimensional model, the first 12 basis functions for u_1, u_2, and θ are kept, so the system given by Eq. (20) has a dimension of 60, 12 for each of the variables u_1, u_2, v_1, v_2 and θ each. A standard ODE integrator (ode45 in Matlab) is applied to simulate the state evolution.

The mechanical loadings now are $f_x = f_y = 6000\sin(\pi t/6)$, and the simulation is performed within the same time interval. The simulated distributions of e_2 and θ from the low-dimensional model are presented in the top row of Fig. 3. The simulated distributions clearly indicate the mechanically induced phase transformation, and the temperature oscillation driven by the mechanical loads due to the thermomechanical coupling. To show the effect of transformation, the distribution of e_2 at $t = 3$ and $t = 9$ from the low-dimensional model is presented in the middle row of the figure. In this case, the entire patch is divided into two sub-areas, associated with the two martensite variants. The combination of the two martensite variants also depends on the loading direction [12]. To demonstrate the thermo-mechanical coupling, the temperature distributions θ at $t = 3$ and $t = 9$ also plotted in the figure (the bottom row). It can be observed that after the transformation, the temperature distribution of the patch is also changing.

To validate the low-dimensional model, a more detailed comparison between the two sets of numerical results (from the PDE model and POD model) is carried out here. To do so, three points in the shape memory alloy patch are chosen, and the strain and temperature values from the two models are compared at these points. The first point is chosen close to the left boundary as $(0.067, 0.5)$, the strain (left) and temperature (right) evolutions at the point during the loading process are presented in the top row of Fig. 4. The second point is chosen close to the center of the patch as $(0.5, 0.63)$, and the strain and temperature evolutions are presented similarly in the middle row of the figure, while those for the third point $(0.75, 0.25)$ are presented in the bottom row. At all the three points, the

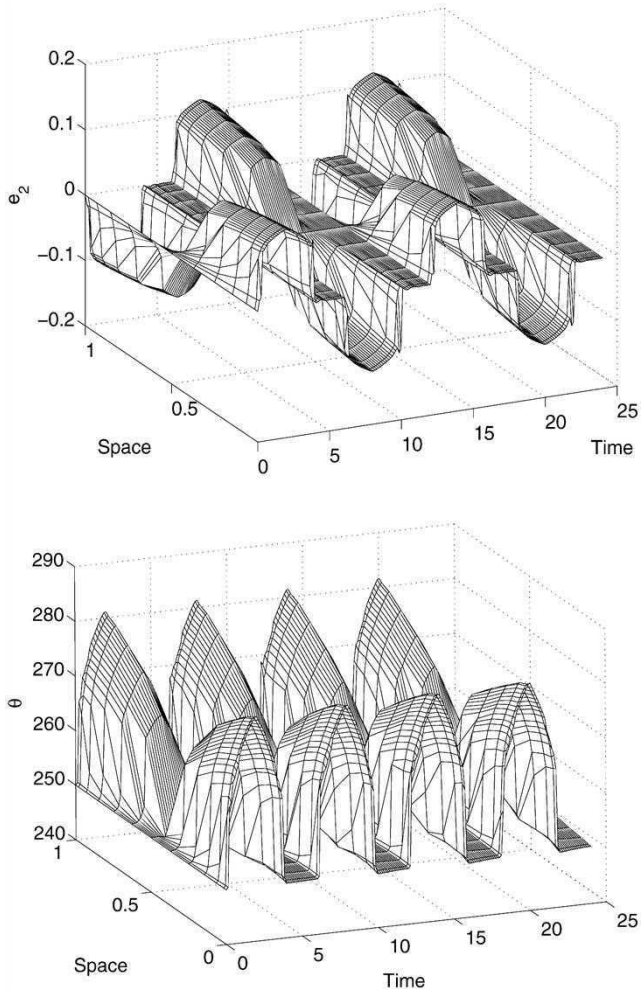

Fig. 1. Simulated evolution of strain and temperature on the central horizontal line in the patch involving phase transformation, using PDE model. (Top) strain evolution; (Bottom) temperature evolution.

strain evolutions simulated using the low-dimensional model agree very well with those from the PDE model, the discrepancies can be distinguished only by a close look at the plots. The phase transition is indicated clearly by the strain evolution.

The temperature evolutions from the low-dimensional model at the three points also agree qualitatively with their counterparts from the PDE model, the oscillatory behaviors of the temperature driven by the mechanical loadings due to the thermo-mechanical coupling are also successfully captured in the low-dimensional model. The agreement is not perfect in temperature evolutions, there are certain discrepancies between the two models. This can be explained as follows. In the dynamics of the patch, the thermal and mechanical fields are coupled in the PDE model, but for the low-dimensional model it is not practical to extract the eigenmodes for the thermal and mechanical fields simultaneously by using the collection matrix including both temperature and displacement distributions, because their magnitude is very different (250 versus 0.1), and characteristics of the variable with smaller magnitude will be ignored if one do so. In the current paper, the eigenmodes for the displacement distributions are obtained by the POD analysis using the collection matrix of displacements only, and similarly for the eigenmodes of temperature distributions. With this simplification, some characteristics associated with the coupling between the thermal and mechanical fields are lost. This loss will induce minor errors in the low-dimensional approximation. When the dynamics of the patch are simulated using the low-dimensional model with a mechanical loading, the characteristics of the thermal behavior driven by the mechanical loading can be captured, but the minor error due to the partly loss of coupling characteristics

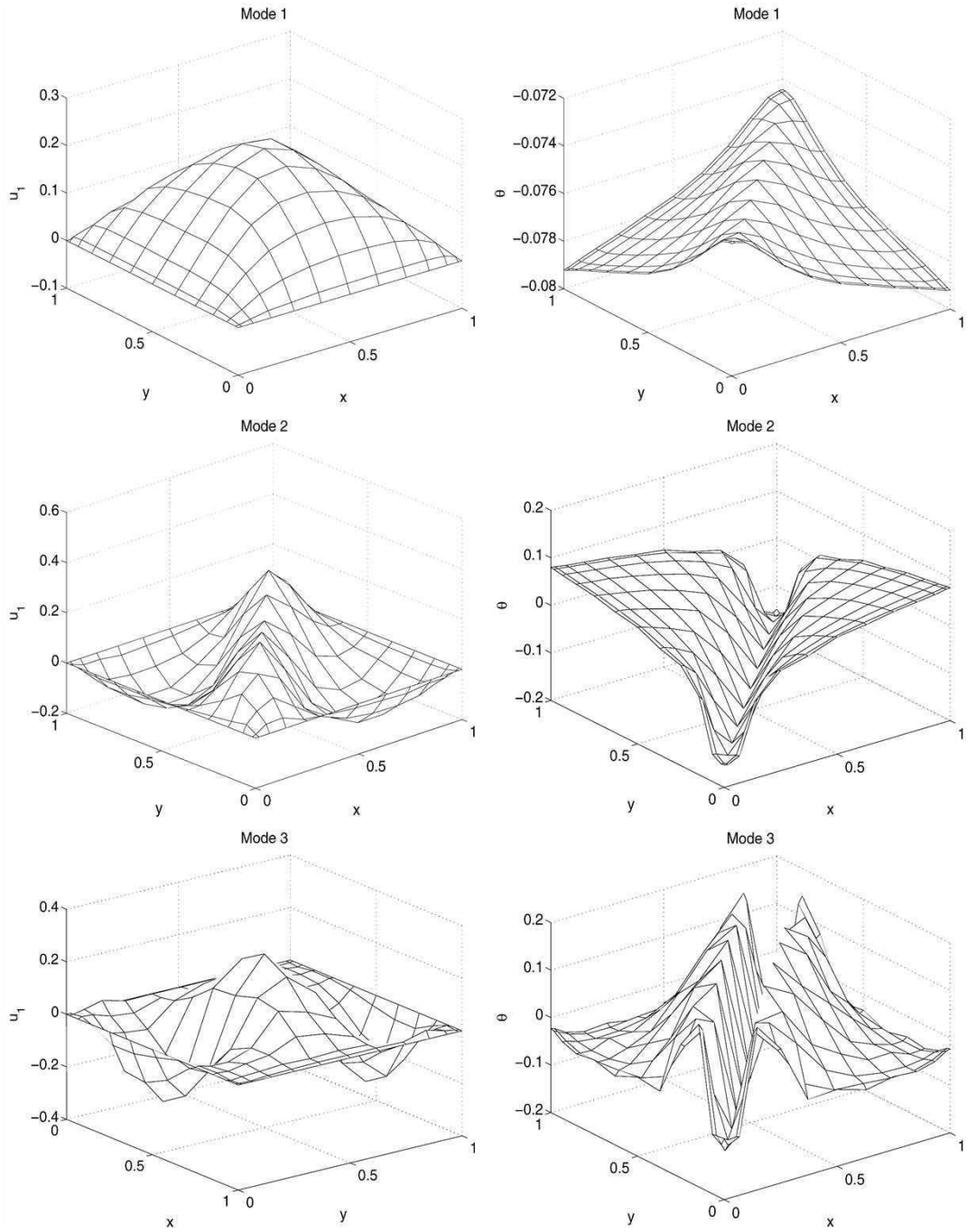

Fig. 2. The first three eigenmodes for u_1 and θ obtained from POD analysis using collection matrix constructed by numerical results of PDE model.

will be accumulated and make the temperature evolutions slightly different from those of the PDE model, just as indicated by the comparison in Fig. 4.

From the above numerical experiments and comparison, it is clearly shown that the low-dimensional model is able to capture the characteristics of the dynamics involving phase transformation, as well as the thermo-mechanical coupling.

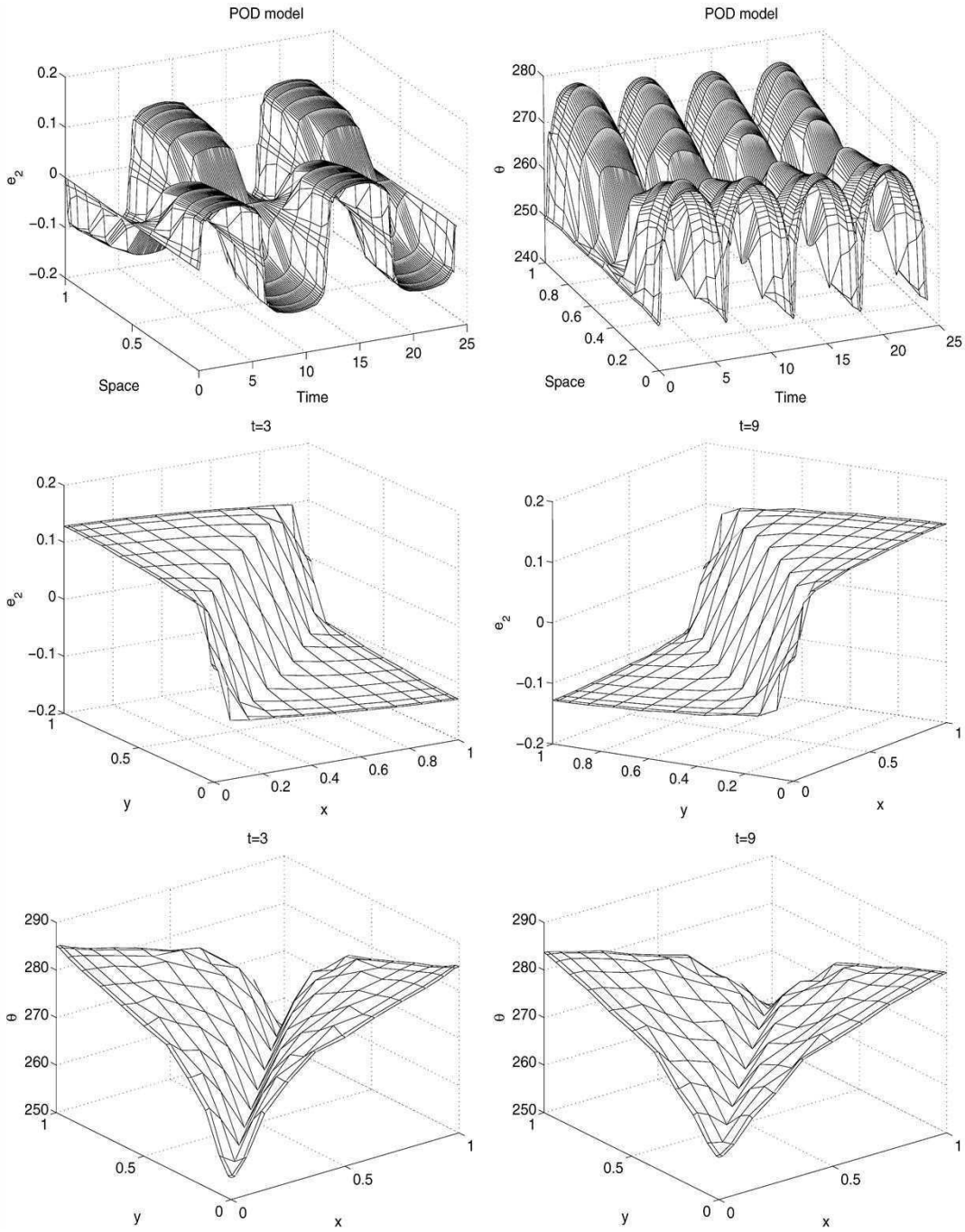

Fig. 3. Numerical simulation of the dynamics of a shape memory alloy patch using a low-dimensional model. From top to bottom, left to right, (a) strain evolution on the central horizontal line, (b) temperature evolution on the central horizontal line, (c) strain distribution at $t = 3$, (d) strain distribution at $t = 9$, (e) temperature distribution at $t = 3$, (f) temperature distribution at $t = 9$.

5. Conclusion and discussion

In this paper, the dynamics of a ferroelastic patch exhibiting square to rectangular martensite transformations has been analyzed. The system of PDEs based on the Landau theory of phase transition has been analyzed numerically by the Chebyshev collocation method. The proper orthogonal decomposition has been employed to extract the eigen-

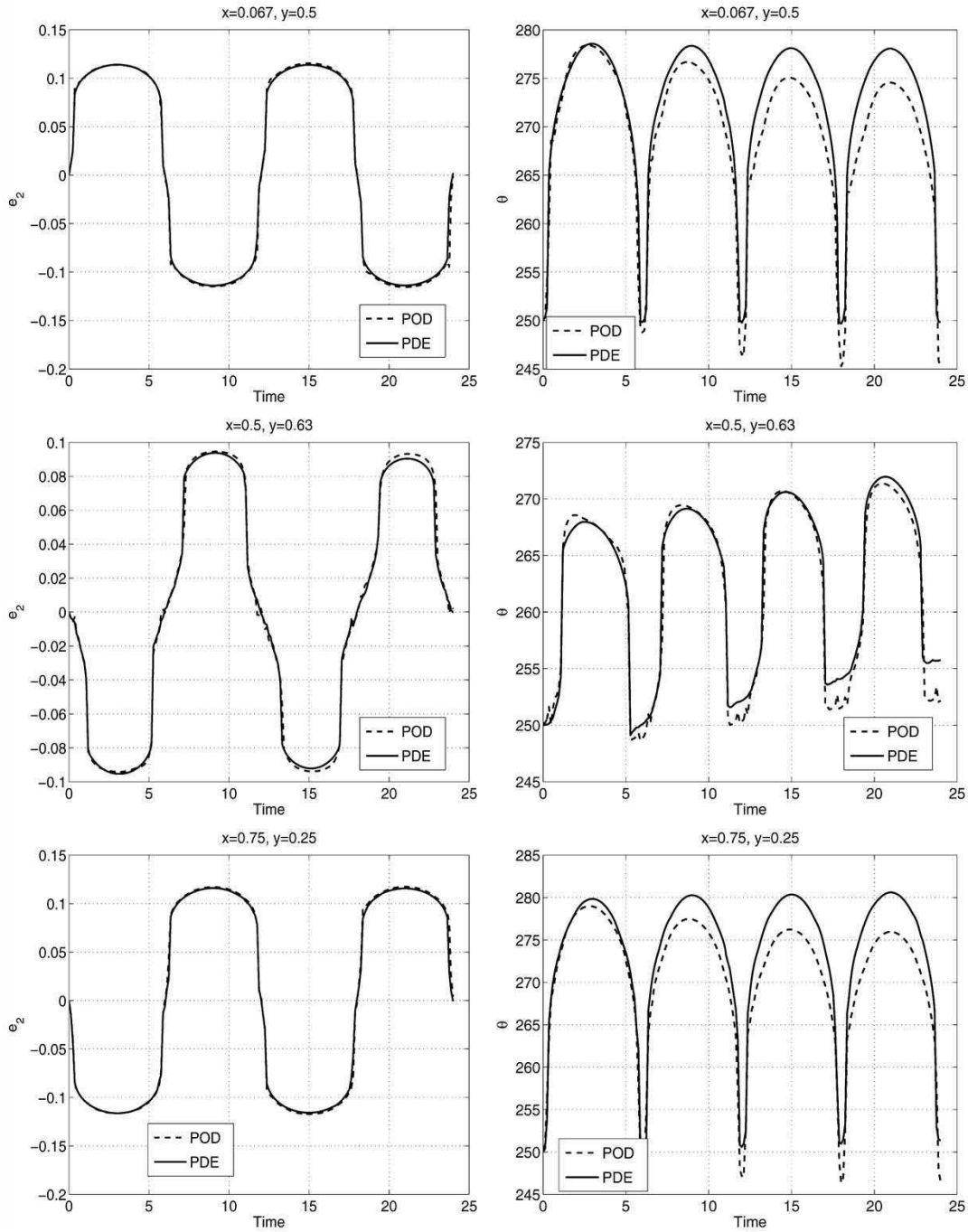

Fig. 4. Comparison of numerical results from the low-dimensional model with those from the PDE model. From top to bottom, left to right, (a) strain evolution at $(0.067, 0.5)$, (b) temperature evolution at $(0.067, 0.5)$, (c) strain evolution at $(0.5, 0.63)$, (d) temperature evolution at $(0.5, 0.63)$, (e) strain evolution at $(0.75, 0.25)$, (f) temperature evolution at $(0.75, 0.25)$.

modes of the dynamics of the patch. A low dimension system has been constructed by projecting the PDEs system onto the subspace spanned by the first few eigenmodes.

Numerical experiments demonstrated that the complicated dynamics of ferroelastic materials can be modeled successfully with the derived low-dimensional system.

References

[1] Q. Alfio, S. Riccardo, S. Fausto, Numerical Mathematics, Springer-Verlag, Berlin, 2000.
[2] P. Homes, J.L. Lumlay, G. Berkooz, J.C. Mattingly, R.W. Winttenburg, Low-dimensional structure in coherent structures in turbulence, Phys. Rep. 287 (1997) 337–384.
[3] T. Lookman, S.R. Shenoy, K.O. Rasmusseh, A. Saxena, A.R. Bishop, Ferroelastic dynamics and strain compatibility, Phys. Rev. B 67 (2003) 024114–024140.
[4] R. Melnik, A. Roberts, K. Thomas, Phase transitions in shape memory alloys with hyperbolic heat conduction and differential algebraic models, Comput. Mech. 29 (1) (2002) 16–26.
[5] R. Melnik, A. Roberts, K. Thomas, Coupled thermomechanical dynamics of phase transitions in shape memory alloys and related hysteresis phenomena, Mech. Res. Comm. 28 (6) (2001) 637–651.
[6] M. Niezgodka, J. Sprekels, Convergent numerical approximations of the thermomechanical phase transitions in shape memory alloys, Numer. Math. 58 (1991) 759–778.
[7] M. Rathinam, L.R. Petzold, A new look at proper orthogonal decomposition, SIAM J. Numer. Anal. 41 (5) (2003) 1893–1925.
[8] C.W. Rowley, T. Colonius, R.M. Murray, Model reduction for compressible flows using POD and Galerkin projection, Phys. D 189 (2004) 115–129.
[9] J. Qiu, J. Tani, D. Osanai, Y. Urushiyama, High-speed actuation of shape memory alloy, in: D.K. Sood, R.A. Lawes, V.V. Varadan (Eds.), Smart Structures and Devices, Proceedings of SPIE, vol. 4235, SPIE, Washinton, 2001, pp. 188–197.
[10] R. Teman, Infinite-Dimensional Dynamical Systems in Mechanics and Physics, Springer-Verlag, New York, 1998.
[11] L.N. Trefethen, Spectral Method in Matlab, SIAM, Philadelphia, 2000.
[12] L.X. Wang, R.V.N. Melnik, Thermomechanical waves in SMA patches under small mechanical loadings, in: M. Bubak, G.D. van Albada, P.M.A. Sloot, J. Dongarra (Eds.), Lect. Notes Comput. Sci., vol. 3039, Springer-Verlag, Berlin, 2004, pp. 645–652.
[13] L.X. Wang, R.V.N. Melnik, Simulation of thermomechanical wave with an empirical low-dimensional model, in: V.S. Sunderam, G.D. van Albada, P.M.A. Sloot, J. Dongarra (Eds.), Lect. Notes Comput. Sci., vol. 3514, Springer-Verlag, Berlin, 2005, pp. 884–891.